Chemical Engineering Journal 393 (2020) 124688

Contents lists available at ScienceDirect

Chemical Engineering Journal

journal homepage: www.elsevier.com/locate/cej

# Efficient CRISPR/Cas9 gene-chemo synergistic cancer therapy via a stimuli-responsive chitosan-based nanocomplex elicits anti-tumorigenic pathway effect

Bing-Chen Zhang[a,1], Peng-Yu Wu[a,1], Jun-Jie Zou[a], Jia-Li Jiang[a], Rui-Rui Zhao[a], Bang-Yue Luo[a], Yu-Qin Liao[a], Jing-Wei Shao[a,b,*]

[a] Fujian Provincial Key Laboratory of Cancer Metastasis Chemoprevention and Chemotherapy, College of Chemistry, Fuzhou University, Fuzhou, Fujian 350116, China
[b] Marine Drug R&D Center, Institute of Oceanography, Minjiang University, Fuzhou, Fujian 350108, China

## HIGHLIGHTS

- Nanocomplex for co-delivery of CRISPR/Cas9 and paclitaxel was constructed.
- The nanosystem triggered efficient gene-editing with good safety.
- The gene therapy of VEGFR2 sensitized the treatment effect of paclitaxel.
- The nanosystem exhibited the synergistic modulation for IL-6-IL-8/NF-κB pathway.
- The nanosystem achieved significant synergistic gene-chemo HCC treatment.

## GRAPHICAL ABSTRACT

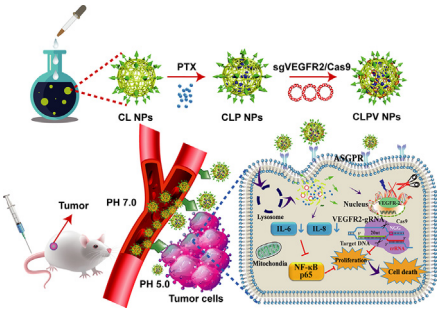


## ARTICLE INFO

*Keywords:*
CRISPR/Cas9 system
Paclitaxel
Co-delivery nanosystem
Gene-chemo synergistic therapy
HCC treatment

## ABSTRACT

Clustered regularly interspaced short palindromic repeat (CRISPR)-associated Cas9 nuclease system (CRISPR/Cas9) has become a powerful toolbox as a gene fixed-point knock-out method and hold the promising prospect for cancer therapy. However, the biological safety of the viral vectors and the instability of exogenous plasmid in blood circulation limits its application. Herein, we reported a lactobionic acid functionalized and stimuli-responsive chitosan based nanocomplex to co-deliver sgVEGFR2/Cas9 plasmid and paclitaxel for hepatoma carcinoma therapy. The genome editing efficiency of sgVEGFR2/Cas9 in the nanosystem achieved up to 38.6% of HepG2 cells *in vitro* and 33.4% of tumor tissues *in vivo*. The nanocomplex suppressed > 60% VEGFR2 protein expression of HepG2 cells and inhibited hepatoma carcinoma (HCC) tumor progress by 70% on mice. *In vivo* study indicated the obvious tumor accumulation and the good biosafety of the nanosystem. Moreover, the gene-drug co-loaded nanoparticles stimulate anti-tumorigenic pathway of HCC by suppressing pro-inflammatory cytokines (IL-6/IL-8) and tumor angiogenesis-related protein (NF-κB p65) expression, which revealed the potential pathway inhibition of PTX when combined with the gene therapy for overexpression VEGFR2 on HCC cells. Overall, this strategy provided a versatile method for high efficiency CRISPR/Cas9 system delivery and showed tremendous application prospect for gene-chemo synergistic therapy.

* Corresponding author at: 2 Xueyuan Road, Sunshine Technology Building, 6FL, Fuzhou University, Fuzhou, Fujian 350116, China.
*E-mail address:* shaojingwei@fzu.edu.cn (J.-W. Shao).
[1] These authors contributed equally to this work.

https://doi.org/10.1016/j.cej.2020.124688
Received 5 October 2019; Received in revised form 22 January 2020; Accepted 6 March 2020
Available online 06 March 2020
1385-8947/ 

## 1. Introduction

Hepatocellular carcinoma (HCC) is one of the aggressive tumors all around the world. With about one hundred and ten thousand people deaths each year in China, the mortality rate ranks the 3rd in malignant tumors of the digestive system, accounting for 45% of the world [1,2]. Paclitaxel (PTX) is an FDA approved chemical drug which has already been used for breast cancer, ovarian cancer and hepatoma in clinical. It has been proved to bind to tumor tubulin so as to regulate tumor cell death [3]. However, PTX treatment of HCC has poor prognosis and is always accompanied by unmanageable sequelae which lead to the neurotoxicity in normal cells [4–6]. In addition, the abnormal over-expression of molecular targets in tumor cells have become the high-profile target for new drug design [7]. These molecular targets include the vascular endothelial growth factor receptor 2 (VEGFR2), which contributes to angiogenesis within the tumor microenvironment and leads to the rapid replication of tumor cells [8,9]. As the non-targeted drug PTX, we surmise that abnormally high expression of tumor-associated molecules may be one of the causes of poor efficacy in the treatment of HCC. Thus, whether combination therapy with gene like VEGFR2 can enhance the efficacy of PTX is needed to explore. To address the issue, the novel gene therapy method of Clustered regularly interspaced short palindromic repeat (CRISPR)-associated Cas9 nuclease system (CRISPR/Cas9) as the gene therapy tool was chosen for the gene-drug combination therapy.

CRISPR/Cas9 has attracted more attention as a mature genome editing technology. It is worked by the appropriate guide RNAs (gRNAs) that direct Cas9 protein to cleave the DNA targets [10–12]. Compared to the siRNA, CRISPR/cas9 technology directly accomplishes the gene knockout in genome and has a better targeting effect [13]. Therefore, editing the specific tumor related molecular targets, the gene therapy technology of CRISPR/Cas9 system holds great potential for cancer treatment. Nevertheless, owing to the instability of lipo-transfection efficiency *in vitro* and the potential danger of viral vector *in vivo*, a major bottleneck for clinic application of CRISPR/Cas9 is the lack of efficient delivery system [14–17]. In recent years, more efficient nano-drug based systems for CRISPR/Cas9 gene delivery have made remarkable progress for tumor targeted therapy compared to the traditional viral vectors [18–20]. Very recently, nanoparticles (NPs) have attached the attention as practical delivery platforms for CRISPR/Cas9 system in view of the great achievements have made in small molecule drugs and antibody proteins. For instant, Peng Wang et al. reported the Cas9 protein and single guide RNA (sgRNA) plasmid co-delivery by lipid-encapsulated gold nanoparticles achieved a good therapeutic effect of melanoma *in vitro* and *in vivo* by suppressing the PIK1 expression [21]. Chao Liang also reported an osteosarcoma (OS) cell-specific aptamer (LC09)-functionalized PEG-PEI-Cholesterol lipopolymer encapsulating CRISPR/Cas9 plasmid encoding VEGFA gRNA and Cas9 [22]. The strategy effectively inhibited OS malignancy and lung metastasis. But the more biodegradable and orientation-release system is still urgent needed for further clinic treatment. Jie Qiao et al. provided using chitosan-coated red fluorescent protein to deliver the CRISPR/Cas9 system. It's provided a more favorable security and long-term effect way for gene editing. The paper proved the ideal gene editing efficiency of nanoplatform *in vitro*. By contrast, we apply the chitosan-based nanocarrier system for the cancer therapy and constructed a novel gene-chemo synergistic treatment nanosystem by co-delivery the traditional chemotherapeutic drugs and CRISPR/Cas9 system. Moreover, we verified the significant gene therapy *in vivo* tumor tissues and improved the tumor-targeting of nanocomplex by modifying specific recognition molecules to reduce the off-targeted risk of CRISPR/Cas9 and side effect of PTX.

Here, we reported a composite nanoparticles of chitosan (CS) loaded with PTX and sg-VEGFR2/Cas9 plasmid (VC) for enhanced cancer therapy (Fig. 1A). CS acted as a practical carrier with special physiological features including non-toxic, excellent biocompatibility and biodegradable characteristics as well as exhibiting pH-responsive effect and sustained drug release profiles when apply to the cancer therapy [23–25]. The proposed approach combined the CRISPR/Cas9, the down-regulation of VEGFR2 expression would be useful for the treatment of non targeted drugs PTX by the co-delivery nanosystem. In addition, β-galactose-carrying lactobionic acid (LA) was conjugated to CS as a targeting moiety to specifically target HCC cells that expressed asialoglyco protein receptors (ASGPR) on their membrane surface [26]. By using the ASGPR targeted CS nanoparticles for co-delivery of anti-cancer drug PTX and VC (CS-LA/PTX/VC, CLPV NPs), we expected to increase uptake of agents in tumors to reduce side effects in normal tissues. The synergistic therapy and gene editing efficiency for HCC was investigated both *in vitro* and *in vivo*. In addition, we evaluated the biosafety and the action-mechanism of CLPV NPs for its influence on the tumorigenic-related pathway (IL-6/IL-8-NF-κB p65), which was active on tumor microenvironment to facilitate the progression of HCC [27]. The research results observed were expected to further gene-chemo therapeutic applications.

## 2. Results and discussion

### 2.1. Preparation of CRSIPR/Cas9 system for VEGFR2 gene editing

Since it has been demonstrated that the exogenous gene transfection efficiency was stable in VEGFR2 overexpression HeLa cells [28], the HeLa cells were used as an *in vitro* cell model to verify the gene editing efficacy of the constructed recombinant plasmid (Fig. 1B). We designed three sgRNAs that could target different sites of the VEGFR2 coding sequence (Table S1). The result showed that sg1/3 recombinant plasmid could down-regulate the VEGFR2 protein levels on the HeLa cells, and the sg1-VEGFR2/Cas9 plasmid had the higher expression inhibition (Fig. S1). Meanwhile, T7 endonuclease 1 (T7E1) assay of HeLa cells and HEK293T cells treated with sg1/3 recombinant plasmids lipo-transfection showed the same conclusion that sg1-VEGFR2/Cas9 plasmid (VC) got the better gene editing efficiency (Fig. S2). The decreased expression of VEGFR2 as a result of the gene knock-out caused by VC, which would be used for gene-chemo composite system. Afterwards, the plasmid with the scramble sequence was prepared as the control, which couldn't inhibit the VEGFR2 expression. By contrast, the mRNA level of VEGFR2 gene continued to decrease from the increasing time for 6 ~ 48 h after the VC transfection (Fig. S3).

### 2.2. Preparation and characterization of CLPV NPs

CS-LA was synthesized by EDC/NHS amide coupling reaction which was characterized by the infrared spectrum that CS-LA had a new peak of amide at 1635 $cm^{-1}$ (Fig. S4). The CL NPs as the carrier with the smallest particle size of 165.5 ± 8.2 nm was prepared at first by changing the stir time (Table S2). By optimizing the ration of CL NPs and PTX, the mass ration of 1:3 for CLP NPs was the better choice to get the good particle size (206.2 ± 4.9 nm) as well as the PTX encapsulation efficiency and drug loading were 44.13% and 67.89% separately (Table S3). Subsequently, the co-delivery system loading both of PTX and VC of CS-LA/PTX/VC (CLPV NPs) was prepared. Except for the nanocomplex for loading 300 μg/mL of VC, the other groups had the ideal particle size range. The plasmid encapsulation efficiency was higher than 90% for the groups of 100, 200 and 300 μg/mL by centrifugation to calculate the free plasmid remaining in the solution (Table S4). As the result proved, the agarose gel electrophoresis experiment not only verified the result of encapsulation efficiency in several of groups, but confirmed the conjugation of VC to the nanoparticles by blocking phenomenon compared to the free VC plasmid was forced through the pores of the gel (Fig. S5). Finally, with the mass ration of 1:3:3 CLPV NPs with the particle size of 238.2 ± 3.8 nm was constructed. As the group of VC delivery only, CLV NPs (216.7 ± 7.4 nm) was prepared for the same mass, and the same

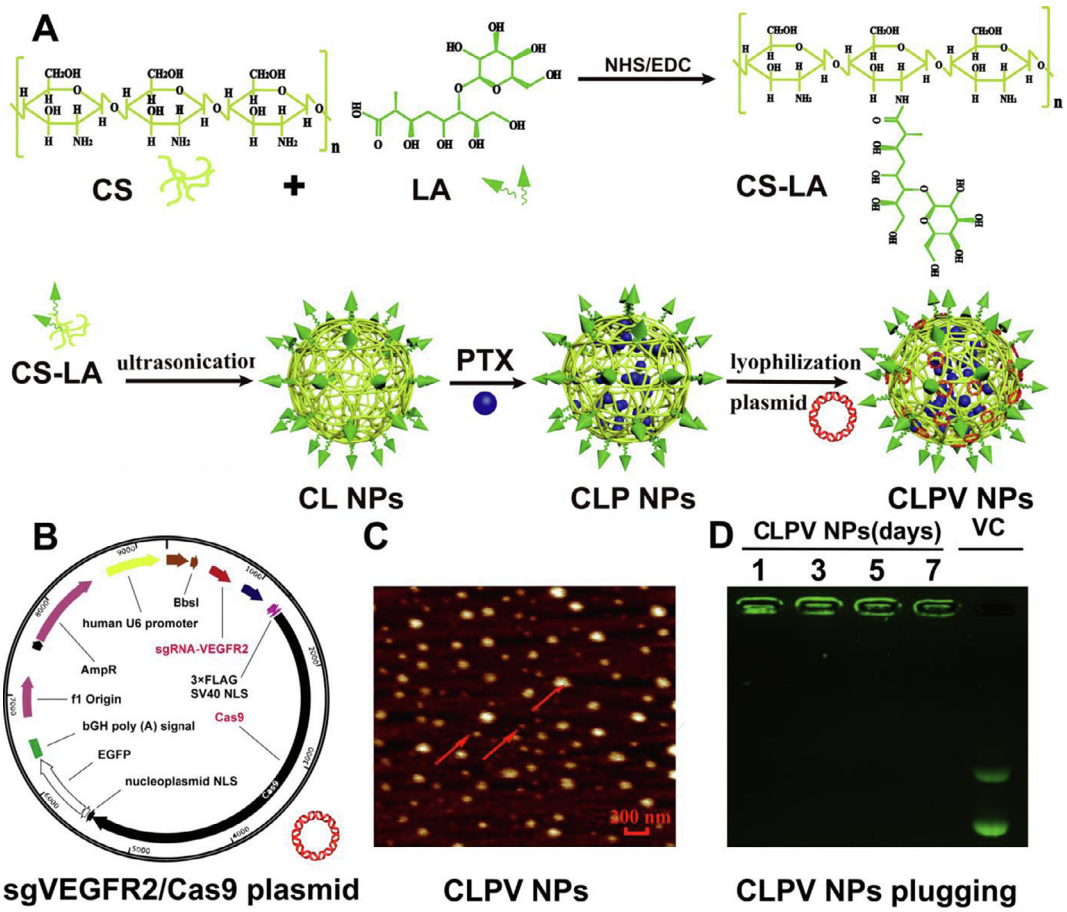


**Fig. 1.** Schematic illustration for preparation of CLPV NPs and relative characterizations. (A) Schematic illustrating the constructed route of CLPV NPs. (B) Plasmid profile of recombinant sgVEGFR2/Cas9 (VC). (C) AFM-image of CLPV NPs with average size about 238.2 nm. (D) Agarose gel electrophoresis experiment to make sure the stability of VC in nanoparticles.

plasmid containing scramble target sequences was used as the control for the nanosystem, which named CLV* NPs (205.1 ± 3.6 nm) and CLPV* NPs (241.6 ± 8.2 nm). These optimized nanoparticles was chosen for the study afterwards, the particle diameter and zeta potential were shown in Fig. S6. In addition, the CLPV NPs were detected by UV spectrum, we found both the UV absorption of PTX and plasmid were observed in composite NPs (Fig. S7). The structure of joint nanoparticles was similar to the spherical according to the AFM image (Fig. 1C).

### 2.3. The drugs release and stability in nanosystem

Chitosan has active amino group on the molecular chain, which can be protonation at acidic pH, increasing its water solubility to release the drugs [29]. To imitate the tumor and normal physical environment, we investigated the ability of nanoparticles to release PTX under the pH 7.4 and 5.5 for 48 h at 37 °C *in vitro*. As shown in Fig. S8, compared with the free drug group, the nanodrug group exhibited a good sustained release profile and pH-responsive. The release rate of PTX alone at pH 7.4 and pH 5.5 was 87.8%, 92.6% respectively, while the PTX from CLP NPs at pH 7.4 and pH 5.5 was 41.4%, 58.2% respectively after 12 h. The pH-responsive release profile of CS was verified on account of the PTX release rate in the tumor acid environment was significantly higher than the normal physical environment. Moreover, the stability of CLPV NPs *in vitro* was evaluated. The particle size was measured once per 12 h after CLPV NPs was dissolved in different solvents (Water, PBS, Cell medium-10%FBS). Cell medium-10% FBS was used to investigate the stability of nanodrug after injection *in vivo*, and the VC had good stability in CLPV NPs within 7 days by gel electrophoresis (Fig. 1D). Meanwhile, considering the zeta potential of CLPV NPs was negative after loading the VC, we investigated the stability of CLPV NPs for incubation with DNase. The experiment indicated VC was avoiding of the degradation by DNase in nanosystem (Fig. S9). There results showed that the CLPV NPs was able to maintain the composite system, suggesting a good stability of the prepared nanoparticles.

### 2.4. Hemolytic experiment and immunogenicity evaluation of nanosystem

If the nanocomplex had hemolytic effect and strong immunogenicity, it would be inducing the great harm to the body. With the dd$H_2O$ as the positive control, the mean fluorescence intensity was measured to determine the degree of the destabilizing effect of red blood cells (RBC). The hemolysis ratio of CS and NPs groups were < 5% and pictures were similar to the PBS group (Fig. S10). Subsequently, Raw264.7 cells was performed to detect the immunogenicity of nanosystem on IL-1β and IL-6 expression. The results showed that all of the groups didn't induce the high expression of cytokines, indicating it didn't cause the inflammatory response of body (Fig. S11). These results proved the ideal biosafety and biocompatibility of CLPV NPs in the physiological environment.

### 2.5. Cellular uptake of gene-chemo drugs

In order to verify cellular uptake efficiencies of nanoparticles for LA-modified targeted delivery of PTX, CLPV NPs was labeled with the FITC which would be captured by confocal microscope with emitting green

fluorescence. We chose the ASGPR-negative HeLa cells as the control, the green fluorescence could not be found until incubation for 2 h. By comparison, the intracellular fluorescence indicated that CLPV NPs was internalized by HepG2 cells only after 1 h (Fig. S12). This revealed that CLPV NPs may be better absorbed by the ASGPR-positive cells. To further confirm this conclusion, flow cytometry was used to detect the fluorescence intensity of HepG2 and HeLa cells after incubation with CPV NPs (no LA-modification) and CLPV NPs (Fig. S13). The results of the experiment showed that the uptake of CLPV NPs was increasing more than CPV NPs in HepG2 cells . In ASGPR-negative HeLa cells, there was no statistical significance in LA-modified nanoparticles uptake. Moreover, we constructed ASGPR-overexpressed HeLa cell lines by pCDNA3.1 plasmids and ASGPR-silenced HepG2 cell lines by siRNA (Figs. S14, S15). The results showed that the uptake of CLPV NPs significantly increased compared to CPV NPs in ASGPR-overexpressed HeLa cells, while the uptake of CLPV NPs was significantly decreased and similar to the CPV NPs in ASGPR-silenced HepG2 cells, which were consistent with the images observed by fluorescence microscopy (Fig. S16A, B). This result indicated that enhanced HCC cells targeting of CLPV NPs through the LA modification improved the entry of NPs into the cells. Meanwhile, in addition to the negative control, we used the traditional lipofectamine reagent as a contrast. The same quantity of VC was incubated with cells by transfection, and the green fluorescence intensity of CLPV NPs was higher than the transfection group of both two cells. In conclusion, the result indicated that the nanosystem greatly improved the uptake compared to the lipofectamine, and significantly increased cellular uptake of the drug and VC, the effective targeting could be reducing the side effects of the drug on normal tissues.

### 2.6. In vitro genome editing efficiency of CLPV NPs

The designed VEGFR2-targeted CRISPR/Cas9 plasmid has been proved available to achieve the cleavage of genome DNA. To evaluate the genome editing efficiency of VC in co-delivery nanosystem, we detected the genome DNA of HepG2 cells and HeLa cells after incubated with CLPV NPs. T7E1 assay was used to distinguish the mutant type from wild type, and the percentage was calculated by agarose gel. As the control, lipo-transfection group exerted an indel frequency of 6.2% and 23.8% respectively in difficult to transfect HepG2 cells and in easy to transfect HeLa cells. The nanocomplex system exhibited more powerful genome editing efficiency, which resulted in 38.6% and 29.6% cleavage of VEGFR2 gene than lipo-transfection (Fig. 2B). In addition, we verified the ability of CLPV NPs to down-regulate the protein expression of VEGFR2 in HepG2 cells (Fig. 2C). Compared with the lipo-transfection group, the nanosystem provided the more efficient delivery platform for CRISPR/Cas9 gene therapy.

### 2.7. In vitro cytotoxicity

Human ASGPR-overexpression hepatoma cell lines of SMMC-7721 and HepG2 were used to investigate the cytotoxicity of nanosystem. According to CCK-8 assay experiments, IC50 of PTX, CLP NPs and CLPV NPs in SMMC-7721 were 14.4, 9.6, 5.5 μM, and there were 20.2, 6.7, 1.6 μM in HepG2 (Fig. 2D). CLV* NPs and CLPV* NPs without the target sequence had the similar IC50 compared to the CS and CLP NPs respectively, and the nanoparticles with the VEGFR2 target sequence (CLP NPs, CLPV NPs) had better tumor-killing ability under same concentration no matter on the HCC cell lines SMMC-7721 or HepG2. The result showed that the VC exhibited the cytotoxicity on the tumor cells in the composite nanosystem, while the plasmid containing scramble target sequences appeared no cells inhibition. Thus, There were not necessary to use the CLV* and CLPV* for the further research of HCC treatment. In addition, the gene-drug co-delivery system of CLPV NPs exhibited higher cytotoxicity than that of PTX alone delivery system (CLP NPs) on the both of cells. Compared to the concentration of the single drugs group CLP NPs and single gene group CLV NPs at the same toxicity, the combination index (CI) of CLPV NPs $< 1$ revealed that the co-delivery of drug-gene was acting synergistically (Fig. S17). It's indicated the gene therapy of VEGFR2 enhanced the.cytotoxicity of PTX alone, showing the efficient synergistic treatment, and reduced the dose of drug so as to get the less side effect. In addition, the cytotoxicity of CLPV NPs was also investigated in mouse hepatoma H22 cells, which was used to construct the tumor-bearing model for the further experiment, and the result showed that the highest cytotoxicity of CLPV NPs compared to the other groups (Fig. S18). Moreover, the safety of the nanodrugs was investigated on the noncancerous HEK293T cells, the effect of CS and NPs groups on the cell viability were not significant (Fig. S19). Thus, the gene-chemo co-delivery system CLPV NPs had the potential for human tumor therapeutics.

### 2.8. In vitro effects of CLPV NPs on cytokines expression

We also investigated the capability of nanocomplex in tumor-associated cytokines regulation, the cytokines IL-1β, TNF-α, IL-6 and IL-8 were related to the occurrence and proliferation of HCC. The effect of IL-1β and TNF-α expression were much weak with CLPV NPs incubation. (Fig. S20), while we found that IL-8 and IL-6 mRNA expression was decreased (Fig. 2E), which had a close relationship with NF-κB p65 pathway, which also acted as the important roles in the HCC. However, PTX was unable to effectively regulate the expression of NF-κB p65 according to the our previous research. To verify that whether the VEGFR2 gene therapy or the synergistic effect of the co-delivery system played the major roles in the pathway regulation, four experimental groups were seted up: PTX group, CLP NPs, CLV NPs, and CLPV NPs. We investigated the protein expression of NF-κB p65 and phosphorylated protein p65 in HepG2 cells after these groups were treated at the same concentration (3 μM PTX、2.5 μg/mL VC) for 24 h. The result of experiments showed that regulation of VEGFR2 by CLV NPs affected the NF-κB p65 expression, while the CLPV NPs more significantly down-regulate the expression of NF-κB p65 and phospho-NF-κB p65 protein in HepG2 cells (Fig. 2F). Compared to the individual treatment group, PTX combined with gene therapy had the synergistic effect on regulating NF-κB p65. These results verified that the joint system is capable of inhibiting tumorigenic relevant pathway (IL-6/IL-8-NF-κB p65). We hypothesize that the overexpression of the VEGFR2 gene affects the therapeutic effect of PTX, and that knock-out of the gene stimulates PTX to achieve synergistic inhibition in the pathway, which will be further verified in animal experiments.

### 2.9. In vivo anticancer activity of CLPV NPs

The tumor inhibitory effect of CLPV NPs *in vivo* was evaluated on H22-bearing model mice (Fig. 3A). As one of the most commonly used mouse transplantable tumor cell lines, H22 is liver cancer cell line that from of C3H mice, which was often used to establish hepatoma models. The subcutaneously inoculated hepatoma models present the significant reaction characteristics of primary tumors to antitumor agents. Intravenous injection of groups (0.9% NC, PTX, CLV NPs, CLP NPs, CLPV NPs) was performed when the tumors grew to about 50 $mm^3$. The volume of tumors and mice weight were recorded every day for 20 d. PTX had negligible influence on the tumor growth. CLV NPs, CLP NPs and CLPV NPs showed effective inhibition for tumor growth by the average volume and tumor weights. By contrast, CLPV NPs had the most significant therapy effect (Fig. 3B–D). The safety of administration was demonstrated by the result that the body weights of CLPV NPs treated group closely resemble to the levels of control group. Notably, the body weights of CLPV NPs group mice were heavier than PTX alone, proving that CLPV NPs reduced the side effect of PTX (Fig. 3E).

In addition, the biochemical changes of serum were measured to indicate the liver, kidney damage with the wild type mice (WT) as the negative control groups (Fig. 3F, S21). The statistical data of alanine

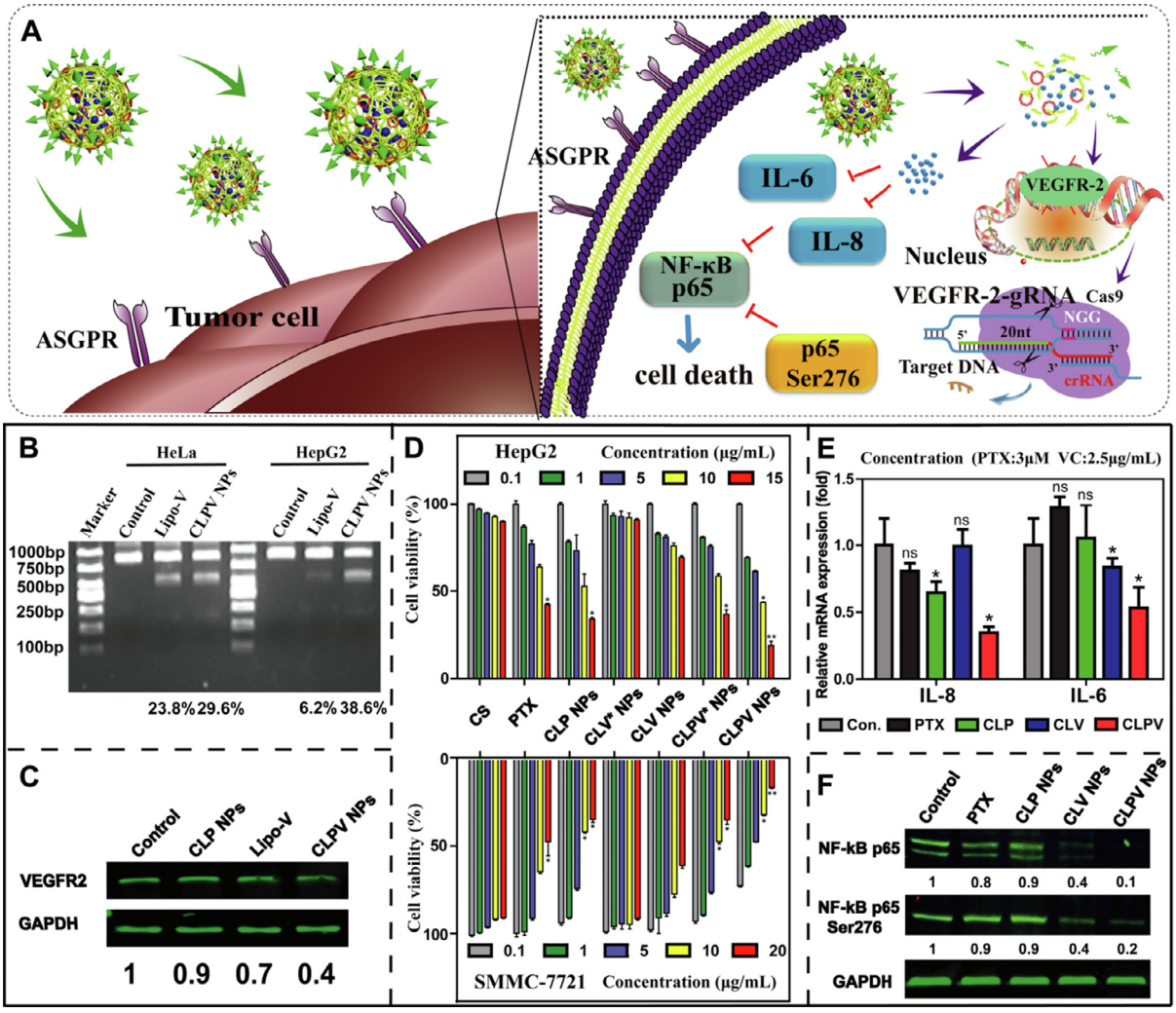


**Fig. 2.** Investigation of HCC treatment efficiency by CLPV NPs *in vitro*. (A) Schematic depiction of HCC treatment by CLPV NPs. (B) T7E1 assays of VEGFR2 gene on HepG2 cells and HeLa cells treated with CLPV NPs and VC lipo-transfection. (C) The VEGFR2 protein expression detection of HepG2 cells after incubated with lipo-transfection and CLP, CLPV NPs. (D) CCK-8 assay for the cytotoxicity of NPs groups compared to the free PTX on SMMC-7721 and HepG2 cell lines. Data are expression as the mean ± standard deviation (SD, N = 6). Note: * P < 0.05, ** P < 0.01. (E) IL-8 and IL-6 mRNA expression and NF-κB p65 protein expression detection by qRT-PCR and WB. Data are expression as the mean ± standard deviation (SD) (N = 6). Note: * P < 0.05. (F) NF-κB p65 and Ser276 phosphorylated protein expression detection of HepG2 by WB with PTX and NPs groups incubation.

aminotransferase (ALT), aspartate transaminase (AST), blood urea nitrogen (Bun), creatinine (Cre) of positive control (tumor-bearing mice, TB) and free PTX group were significant increased compared to the WT group, indicating the functions of liver and kidney in model mice were damaged. Nevertheless, the relative values in each NPs group, especially in CLPV NPs were significant reduced compared to the TB group and PTX group, which indicated that the nanosystem decreased the organs damage from the cancer and the drugs. Moreover, the blood biochemical analysis was further performed by detecting the values of the white blood cells (WBC), RBC, hemoglobin (HGB) and platelets (PLT). Except that there was no significance in RBC counts between all of the groups, TB group exhibited the significantly higher or lower statistical data compared to the normal mice, indicated that the mice were in an abnormal physiological condition. It's worth noting that the statistical data of WBC counts showed the strong immunosuppression of PTX, while the CLPV NPs alleviated this side effect in treatment. Meanwhile, the statistical data of HGB and PLT of CLPV NPs were significant change compared to the TB group and closed to the WT mice. All of the conclusion above revealed the ideal biosafety of the nanocomplex and reduced side effect of the PTX *in vivo* HCC treatment.

### *2.10. In vivo genome editing efficiency of CLPV NPs*

The genome editing efficiency of complex nanoparticles were evaluated by T7E1 assay *in vivo*. CLV NPs and CLPV NPs induced VEGFR2 gene mutation, resulting in an index frequency of 30.2% and 33.4% respectively (Fig. 3G). Sanger sequencing was performed to detect the VEGFR2 gene sites of CLPV NPs treated group. The tumor genomic DNA was extracted to analyze VEGFR2 locus compared to the wild type gene sequence (Fig. S22). The result showed that the VEGFR2 gene alleles mutation at the NGG site of predicted regions, which was the cause of frame shift of VEGFR2 gene in tumor tissue. Thus, this approach could lead to effective gene therapy *in vivo*. Moreover, the VEGFR2 gene and 5 potential off-targeted sites were analyzed because of the high similarity of matching VEFGR2-sgRNA sequence. T7E1 analysis verified that there were no cleavage of 5 potential off-targeted sites and VEGFR2 gene in the normal tissues (Fig. S23). These results from above indicated that CLPV NPs efficient suppressed the HCC tumor progression *in vivo* tissues with low side reaction and had the potential possibility for further clinical treatment.

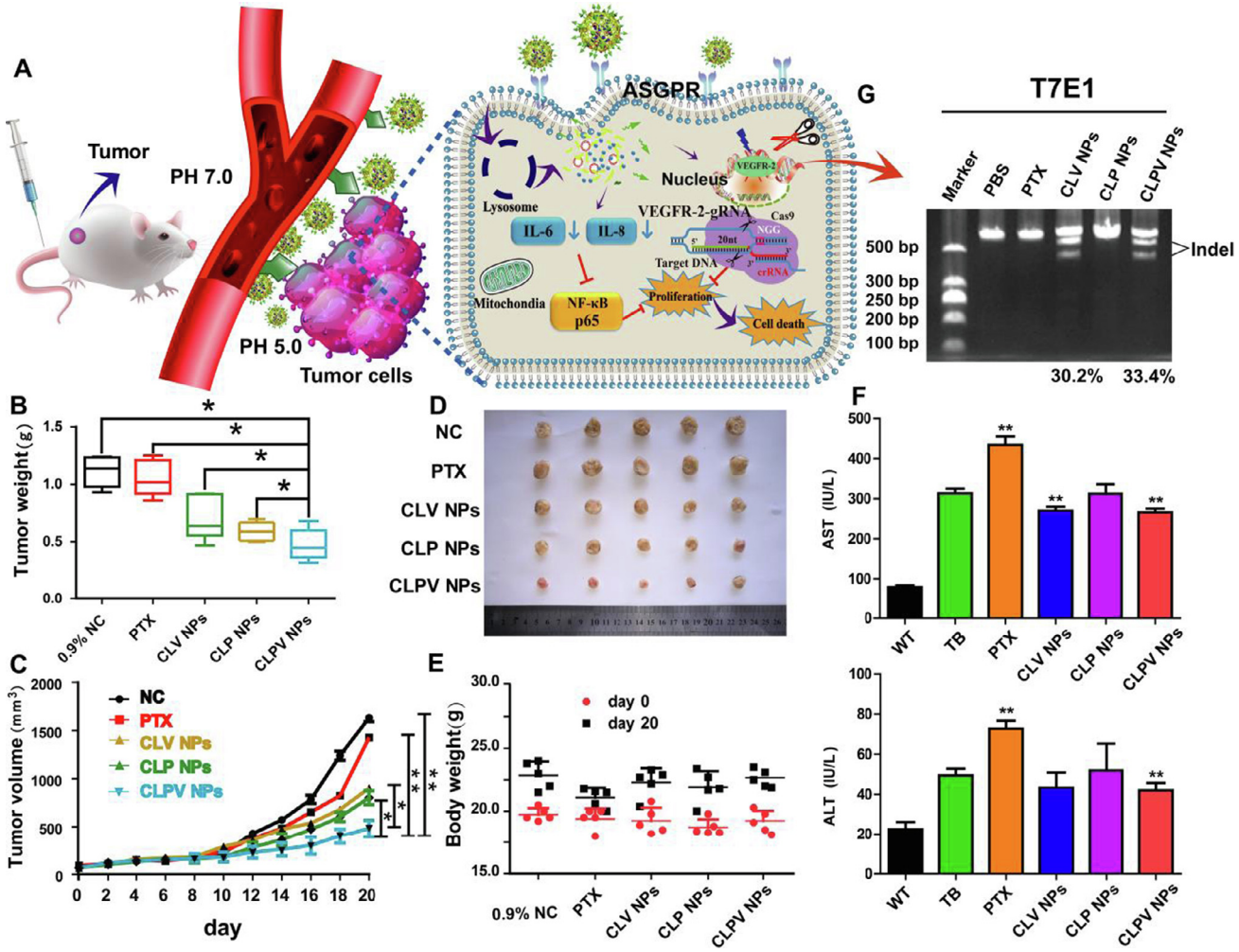


**Fig. 3.** The gene therapy efficiency and HCC treatment efficiency of CLPV NPs *in vivo*. (A) Schematic depiction of HCC treatment by CLPV NPs in tumor-bearing mouse. (B) The excised tumor weights of different formulations after 20 days. (C) The sizes of the tumors recorded each day. Data are expressed as the mean ± SD of five mice in the same group. * P < 0.05, ** P < 0.01.(D) Photographs of the excised tumors from the different groups mice. (E) Body weight of the mice for the first and last day injection. (F) *In vivo* investigation of the biochemical parameters (AST, ALT) in serum of different experiment groups (WB, TB, PTX, CLP, CLV and CLPV NPs). Data are expressed as the mean ± standard deviation (SD). Note: **P < 0.01. (G) T7E1 analysis of the VEGFR2 sgRNA sites on tumor tissues.

### *2.11. In vivo systemic distribution of CLPV NPs and biosafety evaluation of treatment on major organs*

Motivated by the efficient gene editing efficiency and synergistic HCC treatment in tumor-bearing mice, we further explored *in vivo* systemic distribution of CLPV NPs to investigate the tumor targeting of nanosystem. The fluorescence imaging of CLPV NPs labeled with the cy5.5 was detected after injection compared to the free cy5.5 and the fluorescence intensity of the tumor in mice was measured at the same time points. As shown in Fig. 4A, the fluorescence signal was distributed over the whole body during the preliminary 0.5 h, but the obvious accumulation of CLPV NPs had already observed in the tumor compared to free cy5.5 group. Afterwards, the fluorescence concentration increases gradually with time. By contrast, there was no tumor aggregation in the control group, indicating the good tumor targeting of CLPV NPs *in vivo*. Moreover, the fluorescence signal of the control group could not be observed at 12 h, while the CLPV NPs group could still observe the accumulation at tumor tissue at 24 h. The results exhibited the prolonged blood circulation of the nanosystem. The tumor and major organs distribution of free cy5.5 and CLPV NPs after 24 h intravenous injection showed that the CLPV NPs significantly booted the tumor accumulation of nanodrugs, followed by liver and kidneys (Fig. 4B). The fluorescence intensity analysis suggested that the intratumoral average intensity of CLPV NPs was stronger than free cy5.5 at different time points (Fig. 4C, D). All these results indicated that nanosystem achieved efficient drug delivery and enhanced the tumor accumulation.

In addition, the HE staining was performed to investigate the biosafety of the nanocomplex *in vivo* treatment. As shown in Fig. 4E, as similar to the healthy WT mice in the control group, there were no histological morphology change of organs, including the heart, liver, spleen, lung, and kidney after different NPs groups treatments, indicating that nanoparticles had no remarkable side effect on normal tissues. exhibiting the excellent biosafety for the HCC treatment.

### *2.12. In vivo effect of CLPV NPs on regulating tumorigenesis-related pathway*

We also investigated the IL-6-IL-8/NF-κB p65 pathway responses induced by CLPV NPs in tumor tissues. The result was similar to the present study *in vitro*, CLPV NPs exerted good capacity of pathway inhibition by the decreased protein expression of cytokines IL-6 and IL-8 (Fig. S24), and mRNA and protein expression of NF-κB p65 by RNA extraction and nuclear protein extraction were observed significant inhibition on tumor tissues (Fig. S25). PTX and CLP NPs had no significant regulation as well as the negative control PBS group. CLV NPs

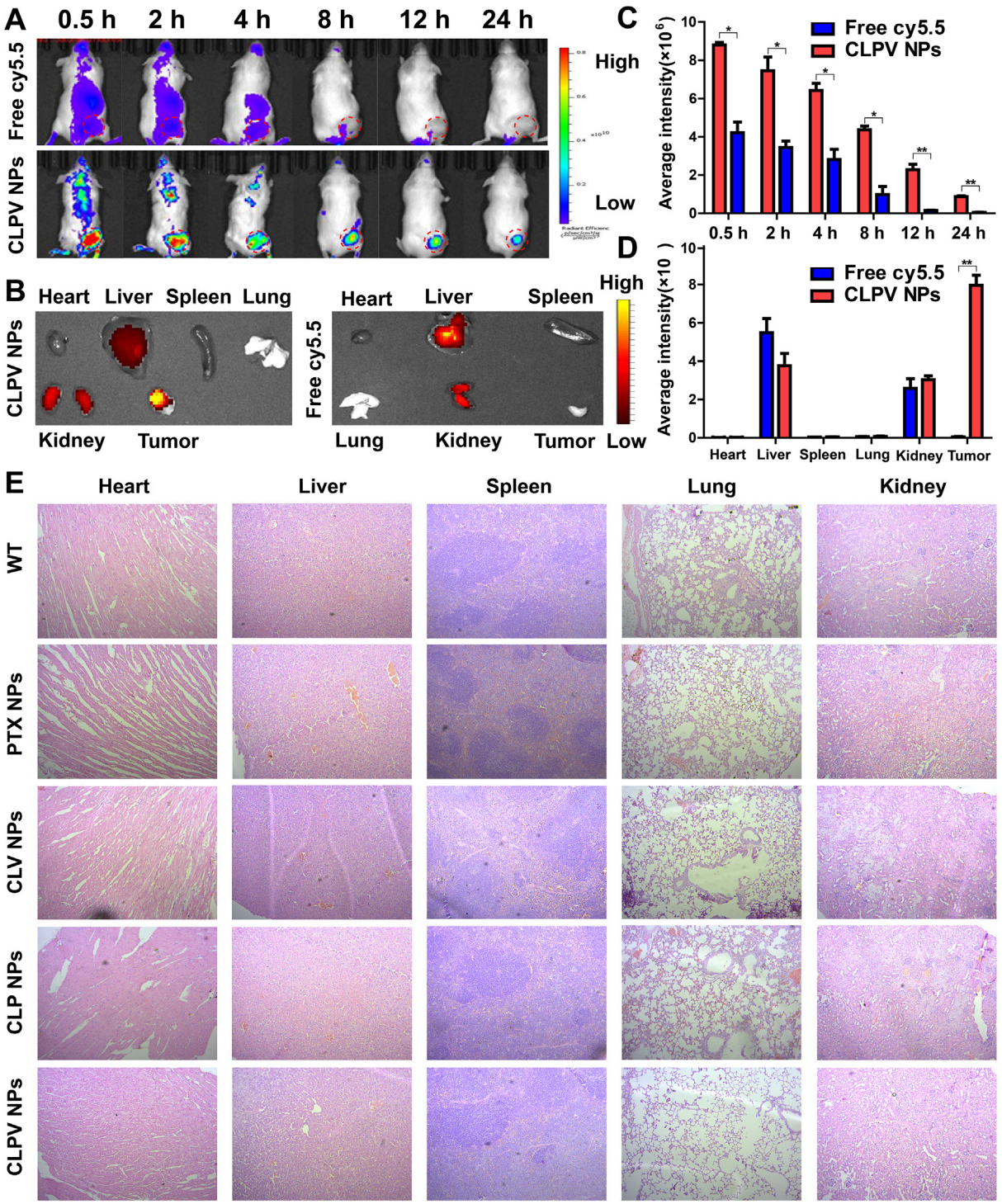


**Fig. 4.** *In vivo* fluorescence imaging of CLPV NPs and HE staining of major organs after treatment. (A) Fluorescence imaging of tumor-bearing mice injected with free cy5.5 and cy5.5-loaded CLPV NPs recorded at 0.5, 2, 4, 8, 12, 24 h. (B) Fluorescence images of the major organs (heart, liver, spleen, lung, kidney) and tumor of two experiment groups above. (C) Average fluorescence intensities of the tumors at indicated time points. (D) Average fluorescence intensities of the major organs and tumors of free cy5.5 and NPs. The data are shown as mean ± SD (n = 3); * $P < 0.05$, ** $P < 0.01$. (E) Photographs of HE-stained major organs after treatment in the tumour model compared to the WT mice.

suppressed the pathway while CLPV NPs showed stronger synergistic effect on regulation. This result verified the point of that the gene therapy of VEGFR2 activated the synergistic effect of PTX on the IL-6-IL-8/NF-κB p65 pathway based on the combination nanosystem. The synergistic inhibition of the pathway could be one of the reason for the more efficient tumor treatment, and worth to further exploration.

## 3. Experimental section

### 3.1. Design of CRISPR/Cas9 system targeting VEGFR2 gene

The recombinant plasmids of CRISPR/Cas9 encoding gRNA of VEGFR2, GFP and Cas9 is originally existed on the template plasmid. We used NCBI to search the nucleotide sequence of human VEGFR2

gene and selected the CDS region to design applicable sequence of VEGFR2-sgRNA. Three sgRNAs were designed according to the Zhang feng research group in case of the inefficient biological activity [30]. The sequences of the three sgRNA is shown at Table S1. The VEGFR2-sgRNA forward and reverse oligo nucleotide sequences were synthesized and BbsI restriction sites were added to the ends during the synthesis. The CRISPR-Cas9 plasmids vector was recombined with double-stranded VEGFR2-gRNA. The ampicillin-resistant LB medium was used to expand the culture of monoclonal strains. Then the positive clones were confirmed by sequence analysis [31]. In addition, the CRISPR-Cas9 plasmid without VEGFR2 knockout functions as the control. The plasmid were extracted to obtain the desired sg-VEGFR2/Cas9 recombinant CRISPR/Cas9 vectors.

HeLa cells were treated with puromycin (1 μg/mL) 24 h after sg-VEFGR2/Cas9 plasmid transfection by LipoFiter$^{TM}$ (Hanheng, Shanghai, China) [32]. After removing the dead cells, remainder cells genome was extracted. The region of genomic VEGFR2 gene (include sgRNA squence, 963 bp) was amplified by PCR using PrimeSTAR Max DNA Polymerase (TaKaRa, Japan). The amplified DNA products was sequenced after recovery.

### 3.2. Synthesis of CS-LA

200 mg chitosan (CS) were dissolved in 0.1% acetic acid under ultrasonic disruption for various time to get more dispersed solutions. The disrupted solutions were stirred at room temperature for further dispersion. Meanwhile, 200 mg lactobionic acid (LA) was dissolved in water and then 600 mg EDC and 600 mg NHS were added into it for activating carboxyl group for 4 h in MES buffer (pH 5.5). Then the activated LA solutions were added into CS solutions with 10 mL MES buffer (pH 5.5) for the conjugate of CS and LA. After 48 h, the mixure was placed in water with dialysis bag (MCW: 8000–14000) for three days. The products were washed 3 times by centrifugation at 12,000 rpm for 30 min. Finally, the products were obtained through freeze-drying [33].

### 3.3. Synthesis of CLP NPs

Firstly, 20 mg CS-LA was dissolved by 0.1% acetic acid undergoing the process of established ultrasonic disruption for further dispersion. Then definite amount of PTX solutions in N, N-dimethyl formamide (DMF) was added drop by drop. The mixture reacted for 48 h at room temperature under vigorous stirring and then transferred to dialysis bag (MCW:8000) to remove DMF and the unloaded PTX. After dialyzing in water for 3 days, the products were obtained by centrifugation at 12,000 rpm for 30 min. After washing 3 times, the products were under cryodesiccation to get the powder.

### 3.4. Synthesis of CLPV NPs

To obtain 100 μg/mL CLP nanoparticles, the finite CLP powder (1 mg) dissolving in 10 mL 0.1% acetic acid was firstly disrupted ultrasonically. Then the corresponding VEGFR2 plasmid (5 mg/ml) solution was added into the appointed CLP NPs according to the established ratio of CS-LA:PTX:VC (1:3:1, 1:3:2, 1:3:3, 1:3:4 and 1:3:5). The mixture were incubated under 25 °C at 120 rpm for 4 h in order to make more combination.

### 3.5. Characterization of CLPV NPs

The amido bond group of CS-LA was characterized via infrared spectrometer. The fundamental properties of prepared nanoparticles including size distribution and zeta potential were determined by Zetasizer Detector. The morphology of CLPV NPs was detected by atomic force microscope (AFM). In order to quantify PTX, the standard curve was established firstly. The ultraviolet absorbance of PTX with various concentrations (5, 20, 30, 40, 45, 50 μmol/L) was detected and the calculated curve was $y = 0.0129x + 0.0371$, $R^2 = 0.9915$. In order to determine the loading capacity of CS-LA, the drug loading efficiency (DL) and encapsulation efficiency (EE) were detected through centrifugation method [34]. The synthetic samples were setted in 50 mL centrifuge tube and then centrifuged at 12000 rpm for 15 min. After that, the supernatant fraction was collected and detected, representing the drug unloaded in CS-LA carriers. The encapsulation efficiency of VC was determined by Ultra Micro Spectrophotometer after the CLPV NPs was centrifuged at 15000 rpm for 30 min at 4 °C. The amount of unloaded free VC in the supernatant of the solution was measured to calculate the encapsulation efficiency compared to the amount of the VC added.

EE-PTX(%) = (Amount of drug added − Amount of drug in supernate)/Amount of drug added × 100%

EE-VC(%) = (Amount of VC added − Amount of VC in supernate)/Amount of drug added × 100%

DL(%) = (Amount of drug added − Amount of drug in supernate)/Amount of nanoparticles × 100%.

### 3.6. Drug controlled release:

To investigate the pH-dependent releasing efficiency of nanocarrier CS, the release rate of free PTX or PTX in CLP NPs were measured. 1 mL PTX or CLP (2.6 mM) was added in dialysis bag (MCW: 12000–14000) and then bags was immersed in 49 mL pH 5.5 and pH 7.4 PBS with 0.5% Tween 80 (v/v). The PBS (pH 7.4) was to simulate neutral value of human normal body fluid and the PBS (pH 5.5) was set to correspond to weak acid value of tumor microenvironment. Under shaking with 150 rpm speed at 37 °C sustainably, 1 mL solution was extracted from these above samples at a ordering time intervals (0, 0.5, 1, 2, 4, 6, 8, 12, 24, 48 h) and the corresponding amount of dialysate medium was supplied [35]. All extracted samples were detected by ultraviolet spectrum and calculated according to the standard curve.

### 3.7. Hemolysis assay

Whole blood was collected from healthy Kunming mice. RBC were obtained by centrifugation at 2000 g for 10 min and washed with PBS for three times. The RBC re-suspended in 1 mL PBS to a concentration of 20% (v/v) and incubated with 0.5 mL NPs (dissolved in PBS) at 37 °C for 2 h, followed by centrifugation at 2000 g for 5 min. The OD value of supernatant after centrifugation was tested at 540 nm. The hemolysis ration of NPs were measured according to the negative control of PBS and positive control of Water.

### 3.8. Cell culture and generation of ASGPR-overexpressed HeLa cell lines and ASGPR-silenced HepG2 cell lines

The cell lines HeLa (human cervical cancer cell line) and HepG2 (human hepatocellular liver carcinoma cell line) cells were purchased from Type Culture Collection of the Chinese Academy of Sciences (Shanghai, China). Both of HeLa cells and HepG2 cells was cultured in DMEM containing 10% fetal bovine serum (FBS). Besides, two type of cells grow with 100 U/mL penicillin G sodium and 100 lg/mL streptomycin sulfate. Cells were maintained at 37 °C in a humidified 5% $CO_2$ incubator. ASGPR-overexpressed HeLa cell lines was prepared by the PcDNA3.1-ASGPR plasmid transfection (2.5 μg/mL). The plasmid was constructed by the CDS sequence of ASGPR with restriction sites of EcoR I and Xba I. ASGPR-silenced HepG2 cell lines was prepared by the ASGPR-siRNA (2.0 μg/mL) transfection and verified by the western blot.

### 3.9. Cellular uptake efficiency

HepG2 and HeLa cells were seeded in a 6-well plate (500,000 per well). CLPV NPs was mixed with the FITC overnight (20 °C, 100r/min). At first, 2.5 μg VC plasmid was transfected by Lipo-transfection. After 10 h, the cells of another group were incubated with the CLPV NPs which contained 2.5 μg plasmids. HepG2 and HeLa cells was collected for 1 h and 2 h respectively, then all of the four groups were stained by Hoechst 33,342 for 15 min, and rinsed with PBS. At last, the cells were measured using a Leica confocal microscope (SP-8, Germany). Emission of Hoechst 33,342 were excited at 405 nm and FITC/GFP were collected at 495 nm respectively [36].

To determine the role of LA binding, beside the HepG2 and HeLa cells were seeded in a 6-well plate (500,000 per well), the group of ASGPR-overexpressed HeLa cells and ASGPR-silenced HepG2 cells were added. At first, 2.5 μg VC was transfected by LipoFiter™ (Hanheng, Shanghai, China). After 10 h, the other two groups were incubated with the CPV NPs and CLPV NPs respectively in four types of cells. The fluorescence intensity of cells was analyzed by flow cytometry after 2 h.

### 3.10. In vitro cytotoxicity experiment and CI measurement of the co-delivery nanosystem

CCK-8 assay evaluated the cytotoxicity of free PTX, CLV NPs, CLP NPs, CLPV NPs on SMMC-7721, HepG2, HEK293T and H22 cells. At fist, cells were cultured on 96-well plates at a density of 5000 cells/well. The cells were incubated for 24 h before the various concentrations free PTX, CLV NPs, CLP NPs, CLPV NPs were diluted with culture medium. Then, cells were maintained at 37 °C for 2 h after CCK-8 solution was added. The amount of CCK-8 formazan product was analyzed spectrophotometrically at 488 nm [37]. Cell viability of all drug concentrations was measured as described by the line graph. The CI of CLPV NPs was calculated from the dose − effect profiles according to the equation: CI = DA/DAm (CLP) + DB/DBm (CLV), where DA and DB are the concentrations of PTX in CLPV NPs and plasmids in CLPV NPs respectively, that in co-delivery system produce a certain level of cytotoxicity, and DAm (CLP) and DBm (CLV) are the concentrations of the single drugs group that produce the same effect.

### 3.11. In vivo experiment:

Murine H22 cells were used to produce HCC models. Female KM mice of 15 g were purchased from Wushi experimental animal trading company (Fuzhou,China). H22 cells suspended in PBS were inoculated in the right hind leg of mice [38] ($1 \times 10^6$ cells/mouse). Expect the normal control group, 20 mice were average divided into four groups (PTX, CLV NPs, CLP NPs, CLPV NPs). treatments on tumor progression. The dose of free PTX and PTX in NPs were 10 mg each mouse, respectively. The mice were treated by intravenous injection every other day when the tumor grew to 50 $mm^3$. The weight of mice and volumes of the tumors were recorded every day. The equation of volumes calculation was that: V ($mm^3$) = 0.5 × length × $width^2$. CLPV NPs was labeled with the cy5.5 using for the *in vivo* imaging. Fluorescence imaging were acquired by Caplier IVIS Lumina at 0.5, 2, 4, 8, 12 and 24 h after the intravenous injection of nanodrugs. Finally, the tumor and major organs were dissected and washed with PBS to obtain the fluorescence images. Serum and blood samples of all groups were collected to evaluate the biochemical indexes, including AST, ALT, Cre, Bun and WBC, RBC, PLT, HGB. The statistical data were measured using reagent kits according the instructions. The major organs of all groups were stained with hematoxylin and eosin and observed with the inverted microscope.

### 3.12. Real-time PCR assay

Compared to the control cells, real-time PCR was used to analyze the relative fold change of IL-6, TNF-α, IL-8 and IL-1β mRNA expression of HepG2 cells after incubated with experiment groups (PTX, CLV NPs, CLP NPs, CLPV NPs). RNA extracted from HepG2 cells using the Trizol reagent (Thermo Fisher, US). The reaction mixture was prepared as follows: 3 μL cDNA (25 ng), 0.2 μL forward primer, 0.2 μL reverse primer and 1.6 μL DEPC water, and then 5 μL SYBR Green qPCR Master Mix (Takara, Japan) was added to 10 μL mixture system. The real-time PCR running program (94 °C for 15 s, 60 °C for 10 s) was repeated by 40 times [39].

### 3.13. Western blot

HepG2 cells or HeLa cells were washed three times by PBS after treated with different of groups for 24 h. Cells were collected in 50 μL of RIPA lysis buffer (Thermo Fisher, US). Each Samples with 30 μg proteins (determined by BCA protein assay kit) were electrophoresed with SDS-PAGE after denaturing in 5 × SDS-PAGE Loading Buffer buffer at 100 °C for 10 min, and then the proteins were transferred to a polyvinyldene difluoride (PVDF) membrane for 1.5 h. After that, the membranes were blocked by 5% BSA. The primary antibodies (diluted 1:500 in BSA) were incubated with membranes overnight at 4 °C after the blots were washed 5 min for three times with TBST. Subsequently, these were washed 10 min for three times with TBST and incubated with IRDye 800CW conjugated secondary antibody (diluted 1:10000 in TBST) for 2 h at RT. Finally, the proteins were observed by Odyssey CLx Western Blot Detection System (Westburg, Netherlands), and the membrane was pictured and calculated by gray-scale statistics [40].

### 3.14. T7 endonnuclease-1 (T7E1) assay

The genome of HepG2 cells and HeLa cells or tumor tissues were extracted after experiment. The region of sg-VEGFR2 sequence was amplified by PCR using VEGFR2-Primer (Table S1). Then PCR products were detected by T7E1 according to the standard protocol [30]. The indel frequency of digestion products were visualized by 1.5% agarose gel, and the genome editing efficiencies were evaluated through the brightness of indel frequency by Image J [41].

### 3.15. Statistical analysis

The detection of particle size, zeta potential and *in vitro* experiments including CCK-8 assay、 qRT-PCR were performed at least three times. Results were expressed as mean ± SD. The *in vivo* experiments, a paired *t*-test was used to compare tumor volume、body weight after nanodrug treatment and control. * $p < 0.05$, ** $p < 0.01$ were considered statistically significant.

## 4. Conclusion

In this study, we firstly developed a CS-LA based gene-drug co-delivery nanosystem composed of sg-VEGFR2/Cas9 plasmid and traditional anti-cancer drug PTX for HCC treatment. The CLPV NPs showed a sustained-release profile and exhibited better cellular uptake ability than free PTX and sg-VEGFR2/Cas9 plasmids alone on HCC cells. The co-delivery of sg-VEGFR2/Cas9 plasmids and PTX nanocomplex showed a synergistic therapeutic effect with CI measurement, and also suppressed > 38% VEGFR2 gene knock-out in HCC HepG2 cells. *In vivo*, CLPV NPs treatment induced > 33% cleavage of targeted genome on tumor tissues and led to > 70% suppression of the tumor progression. The efficient targeting of nanosystem in model mice was verified by the obvious tumor accumulation of *in vivo* fluorescence imaging. The evaluation of biomedical changes (serum, blood) and normal tissues showed the nanocomplex had little toxicity to mice. Moreover, CLPV NPs showed good capacity of synergistic regulation by inhibiting the pro-inflammatory cytokines (IL-6, IL-8) and regulating its downstream tumorigenic pathway (NF-κB p65). Thus, the nanocomplex system not

only showed the high genome editing efficiency for gene therapy, but induced the efficient regulation of tumorigenic pathway for cancer treatment *in vivo*. It's proved the efficient gene-drug synergistic therapy based on the nano delivery system with targeting molecule conjugated. Overall, the CRISPR-Cas9 gene-drug co-delivery nanocomplex system presented a novel strategy for the synergistic cancer therapy.

## Declaration of Competing Interest

The authors declare that they have no known competing financial interests or personal relationships that could have appeared to influence the work reported in this paper.

## Acknowledgment

This project was supported by the National Natural Science Foundation of China (81972832). We thank the Prof. Qi Chen at Fujian Normal University for helpful suggestion and Biomedical Research Center of South China for technical assistance.

## Appendix A. Supplementary data

Supplementary data to this article can be found online at https://doi.org/10.1016/j.cej.2020.124688.

## References

[1] L. Laursen, A preventable cancer, Nature 516 (2014) S2–S3.
[2] C. Schmidt, Immunology: another shot at cancer, Nature 527 (2015) S10–S11.
[3] Z. Li, F. Shan, Y. Wang, et al., Correlation of pathological complete response with survival after neoadjuvant chemotherapy in gastric or gastroesophageal junction cancer treated with radical surgery: a meta-analysis, PLoS One 13 (2018) e0189294.
[4] H. Sadeghi, N. Rahmanian, F.T. Amiri, et al., $^{99m}$Tc-Glucarate for assessment of paclitaxel therapy in human ovarian cancer in mice, Iran. J. Basic Med. Sci. 21 (2018) 77–82.
[5] J. Ferlay, H.R. Shin, F. Bray, et al., Estimates of worldwide burden of cancer in 2008: GLOBOCAN 2008, Int. J. Cancer. 27 (2010) (2008) 2893–2917.
[6] R.H. Mathijssen, A. Sparreboom, J. Verweij, Determining the optimal dose in the development of anticancer agents, Nat. Rev. Clin. Oncol. 11 (2014) 272–281.
[7] A. Ghosh, D. Dasgupta, et al., MiRNA199a-3p suppresses tumor growth, migration, invasion and angiogenesis in hepatocellular carcinoma by targeting VEGFA, VEGFR1, VEGFR2, HGF and MMP2, Cell Death Dis. 8 (3) (2017) e2706.
[8] R.W. Pang, R.T. Poon, From molecular biology to targeted therapies for hepatocellular carcinoma: the future is now, Oncology 1 (2017) 30–44.
[9] T. Hato, A.X. Zhu, D.G. Duda, Rationally combining anti-VEGF therapy with checkpoint inhibitors in hepatocellular carcinoma, Immunotherapy 8 (3) (2016) 299–313.
[10] M. Kaulich, Y.J. Lee, P. Lonn, et al., Efficient CRISPR-rAAV engineering of endogenous genes to study protein function by allele-specific RNAi, Nucleic Acids Res. 43 (2015).
[11] P.D. Hsu, E.S. Lander, F. Zhang, Development and applications of CRISPR-Cas9 for genome engineering, Cell 157 (2014) 1262–1278.
[12] O. Shalem, N.E. Sanjana, E. Hartenian, et al., Genome-scale CRISPR-Cas9 knockout screening in human cells, Science 343 (2014) 84–87.
[13] A. Agrotis, R. Ketteler, A new age in functional genomics using CRISPR/Cas9 in arrayed library screening, Front Genet. 6 (2015) 300.
[14] L. Zangi, N.E. Lui, A. von Gise, et al., Modified mRNA directs the fate of heart progenitor cells and induces vascular regeneration after myocardial infarctio, Nat Biotechnol. 31 (10) (2013) 898–907.
[15] W. Sun, W. Ji, J.M. Hall, et al., Self-assembled DNA nanoclews for the efficient delivery of CRISPR-Cas9 for genome editing, Angew. Chem. Int. Ed Engl. 54 (2015) 12029–12033.
[16] J.A. Zuris, D.B. Thompson, Y. Shu, et al., Cationic lipid-mediated delivery of proteins enables efficient protein-based genome editing in vitro and in vivo, Nat. Biotechnol. 33 (2015) 73–80.
[17] M. Wang, J.A. Zuris, et al., Efficient delivery of genome-editing proteins using bioreducible lipid nanoparticles, Proc. Natl. Acad. Sci. U.S.A. 113 (2016) 2868–2873.
[18] R.J. Platt, S. Chen, Y. Zhou, et al., CRISPR-Cas9 knockin mice for genome editing and cancer modeling, Cell 159 (2014) 440–455.
[19] R.T. Manguso, H.W. Pope, M.D. Zimmer, F.D. Brown, et al., *In vivo* CRISPR screening identifies Ptpn2 as a cancer immunotherapy target, Nature 547 (2017) 413–418.
[20] P. Wang, L.M. Zhang, W.F. Zheng, et al., Thermo-triggered Release of CRISPR-Cas9 System by Lipid-Encapsulated Gold Nanoparticles for Tumor Therapy, Angew. Chem. Int. Edit. 57 (2018) 1491–1496.
[21] P. Wang, L.M. Zhang, Y.Z.Y. Xie, et al., Genome Editing for Cancer Therapy: Delivery of Cas9 Protein/sgRNA Plasmid via a Gold Nanocluster/Lipid Core-Shell Nanocarrier, Adv. Sci. 4 (2017) 1700175.
[22] C. Liang, F.F. Li, F.F. Wang, et al., Tumor cell-targeted delivery of CRISPR/Cas9 by aptamer-functionalized lipopolymer for therapeutic genome editing of VEGFA in osteosarcoma, Biomaterials 147 (2017) 68–85.
[23] K. Jiang, T. Chi, T. Li, et al., A smart pH-responsive nano-carrier as a drug delivery system for the targeted delivery of ursolic acid: suppresses cancer growth and metastasis by modulating P53/MMP-9/PTEN/CD44 mediated multiple signaling pathways, Nanoscale. 10 (13) (2018) 6212–6213.
[24] W. Ou, J.H. Byeon, R.K. Thapa, et al., Plug-and-Play Nanorization of Coarse Black Phosphorus for Targeted Chemo-photoimmunotherapy of Colorectal Cancer, ACS Nano. 12 (10) (2018) 10061–10074.
[25] M. Fathi, S. Majidi, R.K. Zangabad, et al., Chitosan-based multifunctional nanomedicines and theranostics for targeted therapy of cancer, Med. Res.. Rev. 38 (6) (2018) 2110–2136.
[26] G. Zheng, R. Zhao, A. Xu, et al., Co-delivery of sorafenib and siVEGF based on mesoporous silica nanoparticles for ASGPR mediated targeted HCC therapy, Eur. J. Pharm. Sci. 111 (2018) 492–502.
[27] D.P. Chen, W.R. Ning, X.F. Li, et al., Peritumoral monocytes induce cancer cell autophagy to facilitate the progression of human hepatocellular carcinoma, Autophagy 14 (8) (2018) 1335–1346.
[28] L. Hagen, A. Sharma, P.A. Aas, et al., Off-target responses in the HeLa proteome subsequent to transient plasmid-mediated transfection, Biochim. Biophys. Acta. 2015 (1854) 84–90.
[29] R.S. Kalhapure, M. Jadhav, S. Rambharose, C. Mocktar, S. Singh, J. Renukuntla, T. Govender, pH-responsive chitosan nanoparticles from a novel twin-chain anionic amphiphile for controlled and targeted delivery of vancomycin, Colloids Surf B Biointerfaces. 158 (2017) 650–657.
[30] D.A. Scott, F. Zhang, Implications of human genetic variation in CRISPR-based therapeutic genome editing, Nature Medicine. 23 (2017) 1095–1101.
[31] X.F. Ran, P.D. Hsu, J. Wright, et al., Genome engineering using the CRISPR-Cas9 system, Nature Protocols. 8 (2013) 2281–2308.
[32] Z. Meng, Z. Kang, C. Sun, et al., Enhanced gene transfection efficiency by use of peptide vectors containing laminin receptor-targeting sequence YIGSR, Nanoscale. 10 (3) (2018) 1215–1227.
[33] R. Zhao, T. Li, G. Zheng, et al., Simultaneous inhibition of growth and metastasis of hepatocellular carcinoma by co-delivery of ursolic acid and sorafenib using lactobionic acid modified and pH-sensitive chitosan-conjugated mesoporous silica nanocomplex, Biomaterials 143 (2017) 1–16.
[34] K. Jiang, C. Ting, T. Li, et al., A smart pH-responsive nano-carrier as a drug delivery system for the targeted delivery of ursolic acid: suppresses cancer growth and metastasis by modulating P53/MMP-9/PTEN/CD44 mediated multiple signaling pathways, Nanoscale. 9 (27) (2017) 9428–9439.
[35] J. Wang, H. Wang, H. Wang, et al., Nonviolent Self-Catabolic DNAzyme Nanosponges for Smart Anticancer Drug Delivery, ACS Nano. (2019), https://doi.org/10.1021/acsnano.9b01589.
[36] S.M. Kim, S.C. Shin, E.E. Kim, et al., Simple in Vivo Gene Editing via Direct Self-Assembly of Cas9 Ribonucleoprotein Complexes for Cancer Treatment, ACS Nano. 12 (8) (2018) 7750–7760.
[37] Y. Guo, K. Jiang, Z. Shen, et al., A Small Molecule Nanodrug by Self-Assembly of Dual Anticancer Drugs and Photosensitizer for Synergistic near-Infrared Cancer Theranostics, ACS Appl. Mater Interfaces. 9 (50) (2017) 43508–43519.
[38] Y. Liu, G. Zhao, C.F. Xu, et al., Systemic delivery of CRISPR/Cas9 with PEG-PLGA nanoparticles for chronic myeloid leukemia targeted therapy, Biomater Sci. 6 (6) (2018) 1592–1603.
[39] L. Fan, B. Zhang, A. Xu, et al., Carrier-free, pure nanodrug formed by the self-assembly of an anticancer drug for cancer immune therapy, Mol. Pharm. 15 (6) (2018) 2466–2478.
[40] Z. Shen, B. Li, Y. Liu, et al., A self-assembly nanodrug delivery system based on amphiphilic low generations of PAMAM dendrimers-ursolic acid conjugate modified by lactobionic acid for HCC targeting therapy, Nanomedicine. 14 (2) (2018) 227–236.
[41] B. Suresh, S. Ramakrishna, H. Kim, et al., Cell-penetrating peptide-mediated delivery of cas9 protein and guide RNA for genome editing, Methods Mol. Biol. 1507 (2017) 81–89.